

Femtosecond Diffractive Imaging with a Soft-X-ray Free-Electron Laser

Henry N. Chapman,^{1,2,*} Anton Barty,¹ Michael J. Bogan,¹ Sébastien Boutet,^{1,3,4} Matthias Frank,¹ Stefan P. Hau-Riege,¹ Stefano Marchesini,^{1,2} Bruce W. Woods,¹ Saša Bajt,¹ W. Henry Benner,¹ Richard A. London,^{1,2} Elke Plönjes,⁵ Marion Kuhlmann,⁵ Rolf Treusch,⁵ Stefan Düsterer,⁵ Thomas Tschentscher,⁵ Jochen R. Schneider,⁵ Eberhard Spiller,⁶ Thomas Möller,⁷ Christoph Bostedt,⁷ Matthias Hoener,⁷ David A. Shapiro,² Keith O. Hodgson,³ David van der Spoel,⁴ Florian Burmeister,⁴ Magnus Bergh,⁴ Carl Caleman,⁴ Gösta Huldt,⁴ M. Marvin Seibert,⁴ Filipe R.N.C. Maia,⁴ Richard W. Lee,^{1,4} Abraham Szöke,^{1,4} Nicusor Timneanu,⁴ and Janos Hajdu^{3,4,†}

¹ *University of California, Lawrence Livermore National Laboratory, 7000 East Avenue, Livermore CA 94550, USA.*

² *Center for Biophotonics Science and Technology, University of California, Davis, 2700 Stockton Blvd., Suite 1400, Sacramento, CA 95817, USA.*

³ *Stanford Synchrotron Radiation Laboratory, Stanford Linear Accelerator Center, 2575 Sand Hill Road, Menlo Park, California 94305, USA.*

⁴ *Laboratory of Molecular Biophysics, Department of Cell and Molecular Biology, Uppsala University, Husargatan 3, Box 596, SE-75124 Uppsala, Sweden.*

⁵ *Deutsches Elektronen-Synchrotron, DESY, Notkestraße 85, D-22607 Hamburg, Germany.*

⁶ *Spiller X-ray Optics, Livermore CA 94550, USA.*

⁷ *Institut für Atomare Physik, Technische Universität Berlin, Hardenbergstraße 36, PN 3-1, 10623 Berlin, Germany.*

Theory predicts [1, 2, 3, 4] that with an ultrashort and extremely bright coherent X-ray pulse, a single diffraction pattern may be recorded from a large macromolecule, a virus, or a cell before the sample explodes and turns into a plasma. Here we report the first experimental demonstration of this principle using the FLASH soft X-ray free-electron laser. An intense 25 fs, 4×10^{13} W/cm² pulse, containing 10^{12} photons at 32 nm wavelength, produced a coherent diffraction pattern from a nano-structured non-periodic object, before destroying it at 60,000 °K. A novel X-ray camera assured single photon detection sensitivity by filtering out parasitic scattering and plasma radiation. The reconstructed image, obtained directly from the coherent pattern by phase retrieval through oversampling [5, 6, 7, 8, 9], shows no measurable damage, and extends to diffraction-limited resolution. A three-dimensional data set may be assembled from such images when copies of a reproducible sample are exposed to the beam one by one [10].

X-ray free-electron lasers (X-ray FELs) are expected to permit diffractive imaging at high-resolutions of nanometer- to micrometer-sized objects without the need for crystalline periodicity in the sample [1, 2, 3, 4]. High-resolution structural studies within this size domain are particularly important in materials science, biology, and medicine. Radiation-induced damage and sample movement prevents the accumulation of high-resolution scattering signals for such samples in conventional experiments [11, 12]. Damage is caused by energy deposited into the sample by the very probes used for imaging, e.g. photons, electrons, or neutrons. At X-ray frequencies inner shell processes dominate the ionisation of the sample; photoemission is followed by Auger or fluorescence emission and shake excitations. The energies of the ejected photoelectrons, Auger electrons, and shake electrons differ from each other, and these electrons are released at different times, but within about ten femtoseconds, following photoabsorption [1, 13]. Thermalisation of the ejected electrons through collisional electron cascades is completed within 10-100 femtoseconds [14, 15]. Heat transport, diffusion and radical reactions take place over some picoseconds to milliseconds.

Radiation tolerance in the X-ray beam could be substantially extended, if we could collect diffraction data faster than the relevant damage processes [1, 16]. This

approach requires very short and very bright X-ray pulses, such as those expected from short-wavelength free-electron lasers. However, the large amount of energy deposited into the sample by a focused FEL pulse will ultimately turn the sample into a plasma. The question is when exactly would this happen? There are no experiments with X-rays in the relevant time and intensity domains, and our current understanding of photon-material interactions on ultra-short time scales and at high X-ray intensities is, therefore, limited. Computer simulations based on four different models [1, 2, 3, 4] postulate that a near-atomic resolution structure could be obtained by judicious choice of pulse length, intensity and X-ray wavelength, before the sample is stripped from its electrons and is destroyed in a Coulomb explosion. Near-atomic resolution imaging with X-ray FEL pulses faces other formidable challenges that must be addressed, such as developing the ability to record low-noise and interpretable diffraction data under the extreme illumination conditions expected from a focused FEL pulse.

Our experimental demonstration of “flash diffractive imaging” uses the first soft X-ray FEL in the world, the FLASH facility (formerly known as the VUV-FEL) at the Deutsches Elektronen-Synchrotron (DESY) in Hamburg [17]. FLASH generates high power soft X-ray pulses by the principle of self-amplification of spontaneous emission

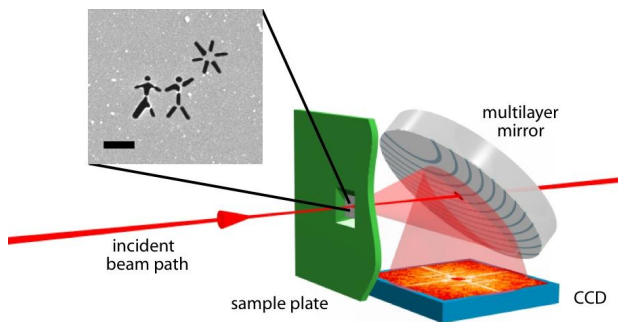


FIG. 1: Schematic diagram of the experimental apparatus. The FEL beam is incident from the left and is focused to a $20\text{-}\mu\text{m}$ spot on the sample, which is a 20-nm thick transmissive silicon nitride membrane with a picture milled through its entire thickness using a FIB (this is enlarged in the inset, and the scale bar indicates $1\text{ }\mu\text{m}$). The direct beam passes through the sample window and exits the camera through a hole in a graded multilayer planar mirror. The diffracted light from the sample reflects from that mirror onto a CCD detector. The contour lines on the mirror depict lines of constant incidence angle (constant multilayer period). The on-axis path length from the sample to the detector is 55 mm . For 32 nm radiation and objects smaller than $20\text{ }\mu\text{m}$, this distance is in the far field, where the diffraction pattern is equal to the Fourier transform of the exit wave [27]. The numerical aperture of the detector is 0.25 .

(SASE) [18]: a relativistic electron pulse from a superconducting linear accelerator makes a single pass through a periodic magnetic field of an undulator. During the high-gain lasing process, the electrons, perturbed by the magnetic field of the undulator and by their own photon field, form coherent micro-bunches, which behave like a single giant charge, producing strong amplification. For our experiment, FLASH was operating in an ultrashort pulse mode [17], resulting in 25 fs coherent FEL pulses with about 10^{12} photons in a pulse.

Figure 1 shows our experimental arrangement. Diffractive imaging is elegant in its simplicity: a coherent X-ray beam illuminates the sample, and the far-field diffraction pattern of the object is recorded on an area detector. We focused a coherent 25 fs X-ray pulse from FLASH to achieve a peak intensity of $(4 \pm 2) \times 10^{13}\text{ W/cm}^2$ on the sample. We recorded the far-field diffraction pattern of the object on a novel detector centred on the forward direction (see Methods). The image information encoded in the coherent diffraction pattern is similar to a hologram [19], except that the object acts as its own scattering reference. Image reconstruction was performed by phase retrieval using our iterative transform algorithm, Shrinkwrap [8] (see Methods). Unlike similar algorithms [7, 20, 21, 22, 23], Shrinkwrap solves the phase problem without requiring any a priori knowledge about the object.

The ultrafast coherent diffraction pattern of a nanostructured non-periodic object is shown in Fig. 2(a).

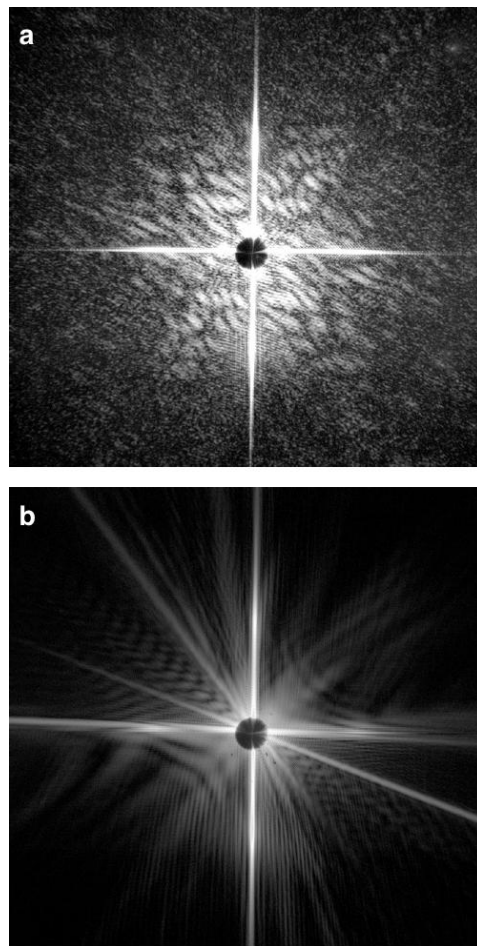


FIG. 2: Flash X-ray coherent diffraction patterns. (a) Coherent diffraction pattern recorded for a single $(4 \pm 2) \times 10^{14}\text{ W/cm}^2$, $25 \pm 5\text{ fs}$ pulse, and (b) for the subsequent pulse of similar intensity and duration, 20 s later, showing diffraction from the damage caused by the pulse that formed (a). The intensity is shown on a logarithmic grey scale with black denoting 1 photon/pixel and white denoting $2000\text{ photons/pixel}$ for (a) and $50,000\text{ photons/pixel}$ for (b). The entire patterns are shown as detected by the CCD, and extend to a diffraction angle of 15° at the midpoint of the edges (corresponding to a momentum transfer of $8.1\text{ }\mu\text{m}^{-1}$).

The object was a micron-sized pattern cut through a partially-transparent silicon nitride membrane with a focused-ion beam (FIB), and it is shown in the insert of Figure 1. The pattern extends to a diffraction angle of 15° at the midpoint of its edge. Based on low-fluence optical parameters [24], we estimate [3, 25] that the absorbed energy density was approximately 20 eV/atom in the silicon nitride and that the sample reached a temperature of about $60,000\text{ }^\circ\text{K}$ before vaporizing. A second diffraction pattern taken 20 s after the first exposure is shown in Figure 2(b). This shows diffraction from a hole left in the membrane caused by the first pulse. That is, the first pulse utterly destroyed the sample but not before a diffraction pattern of the apparently undamaged

object could be recorded. Images of the object obtained with a scanning electron microscope (SEM), before and after FEL exposure, are shown in Figure 3.

The main features of the diffraction pattern of Figure 2(a) are speckles and strong vertical and horizontal lines that pass through the centre of the pattern. The horizontal and vertical lines are caused by interference of the waves diffracting from the opposite edges of the square window frame that holds the silicon nitride membrane. The speckles correspond to two length scales of the sample. The modulations of ~ 60 pixels (measured diagonally) in the diffraction pattern near the centre correspond to the narrow $2.5 \mu\text{m}$ diagonal dimension of the object; and the finer speckles of about 16 pixels correspond to the distance between the picture object and the window frame in which it is centered. The speckles remain well defined out to the edge of the detector, although their visibility diminishes with scattering angle. This may be due to the fact that at the high diffraction angles at the edge of the CCD detector, the optical path difference between rays diffracting from points in the object transversely separated by $20 \mu\text{m}$ (the sample window size) is $\sin(15^\circ) \times 20 \mu\text{m} = 5 \mu\text{m}$. This is comparable to the length of a 25 fs pulse, which is $7.5 \mu\text{m}$. That is, the overlap of the beams in time (and hence interference between them) only occurs for one third of the pulse at high angles.

Figures 3(b) and (d) show the image of the object reconstructed directly from the diffraction pattern of Figure 2(a). The angular acceptance α , of our detector is 15° at the midpoint of the detector edges, and 20° at the corners. The diffraction limited resolution length is $\lambda/(2 \sin \alpha) = 62 \text{ nm}$ for a wavelength of $\lambda = 32 \text{ nm}$. This length is defined as the half-period of the finest spatial frequency in the image, equal to an image pixel width. Along diagonal directions the increased CCD acceptance gives a resolution length of 43 nm. The actual image resolution would be worse than the diffraction limit if the retrieved phases were incorrect, in the same way that phase errors in a lens cause image aberrations. We estimate the image resolution by computing the Phase-Retrieval Transfer Function (PRTF) [9, 23], shown in Figure 4. This function represents the confidence for which the diffraction phases have been retrieved and is calculated by comparing the Fourier amplitudes of the average of multiple independent reconstructions to the measured diffraction amplitudes. Where the phase of a particular Fourier component is consistently retrieved the complex values add in phase, whereas if the phase is random the sum will approach zero. The PRTF is thus equal to unity when the phase is consistently retrieved and zero when the phase is unknown. We use the convention that the resolution is given by the point where the PRTF drops to $1/e$ (reference [23]), which for this image occurs at the resolution limit (62 nm). We note that the same experimental geometry deployed on a hard

X-ray free electron laser operating at 0.15 nm wavelength would yield a diffraction-limited resolution length of 0.3 nm.

The “lensless” imaging method used here can be extended to atomic resolution, which will require shorter wavelength X-rays and tighter focusing than demonstrated here. Hard X-ray FELs are currently being developed that will create pulses which, when focused on the sample, will produce five orders of magnitude higher photon intensities than used here. An understanding of photon-material interactions on ultra-short time scales and at high x-ray intensities is fundamentally important to all experiments with X-ray lasers. This area of science is virtually unexplored. The FLASH free-electron laser in Hamburg is the first radiation source to permit experiments near the relevant photon energies and intensities. Our present results validate the concept of single-shot imaging with extremely intense and ultra short soft X-ray pulses that are capable of destroying anything in their path. The resulting diffraction pattern carries high-resolution structural information about the object, and the resolution of the reconstructed image extends to the diffraction limit. This indicates that significant damage occurs only after the ultrashort 25 fs FEL pulse traverses the sample. These results have implications for studying non-periodic molecular structures in biology, or in any other area of science and technology where structural information with high spatial and temporal resolution is valuable. They also point to the viability of nanometer-to atomic-resolution imaging of non-periodic and non-crystalline objects [1, 2, 3, 4] with hard X-ray FELs.

METHODS

Samples consisted of a 20-nm thick silicon nitride membrane spanning a $20 \mu\text{m}$ wide square silicon window. The pattern was cut through the membrane with a dual-beam focused ion beam instrument (FEL, National Center for Electron Microscopy, Lawrence Berkeley National Laboratory), using a 500 pA beam of 30 keV Ga^+ ions. The 20 nm thick silicon nitride membrane has a transmission of 44% at a wavelength of 32 nm, and causes an estimated phase advance of 20° relative to propagation through the same length of vacuum, calculated from the known low-fluence optical constants [24].

Experiments were performed in vacuo as everything in the direct beam contributes to the diffraction pattern. The samples were placed in a vacuum vessel 70 m from the FEL undulator. The FEL pulse was focused to a $30 \mu\text{m} \times 20 \mu\text{m}$ focal spot on the sample with a 2-m focal length ellipsoidal mirror in the beam line. Single pulses were selected with a fast shutter. Due to the source coherence, no aperture was needed to select a coherent patch of the beam, nor was a monochromator used to select a narrow wavelength band of the radiation.

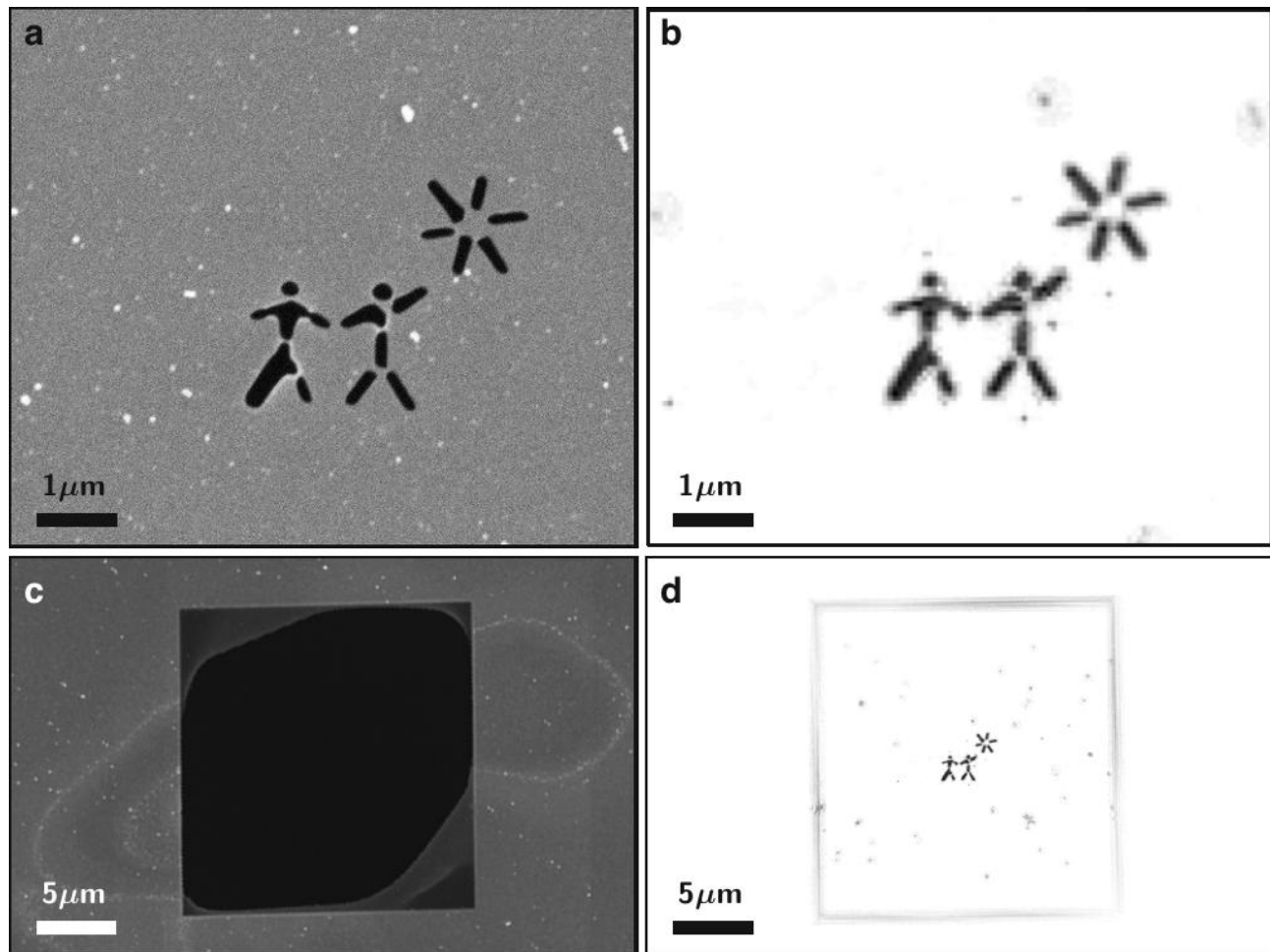


FIG. 3: The reconstructed X-ray image shows no evidence of the damage caused by the pulse. (a) Scanning electron microscope (SEM) image of the sample before exposure to the FEL beam. The 20 nm thick sample was held in a square supporting window that is 20 μm wide. (b) and (d) Image reconstructed, from the ultrafast coherent diffraction pattern of Fig. 2 (a), by phase retrieval and inversion using the Shrinkwrap algorithm [8]. The squared modulus of the retrieved complex image is displayed on a linear grey scale from zero scattered photons/pixel (white) to 1.5×10^6 scattered photons/pixel (black). Pixel size in the reconstruction = 62 nm in (b), corresponding to the half period of the finest spatial frequency that can be recorded on our camera at 32 nm wavelength. The retrieved image clearly shows the silicon window edge (in d), the FIB pattern, and dirt particles. (c) SEM image of the test sample after the exposures to the FEL beam, showing the square 20- μm window and some remaining silicon nitride, as well as visible damage to the silicon support caused by the non-circular beam. The scale bar for (a) and (b) is 1 μm and the scale bar for (c) and (d) is 5 μm .

A novel X-ray camera was developed to record low-noise diffraction data from the sample in the forward direction (see Figure 1). In this camera, a graded multilayer plane mirror separates the diffracted beam from the direct beam, and the intense direct beam passes harmlessly through the hole in the centre of the mirror without damaging the detector. The diffracted light reflects onto a back-illuminated direct-detection CCD chip (Princeton Instruments in-vacuum PI-MTE CCD), containing 1300×1340 square pixels of 20 μm width. The resonant X-ray multilayer of the planar mirror consists of layers of Si, Mo, and B_4C , and was fabricated so that the layer period varies from 18 nm to 32 nm across the mirror. The variation in multilayer period matches the variation

in the angle of incidence of rays emanating from the sample and which strike the mirror. This angle varies from 30° to 60° , as depicted by the contour lines on the mirror in Figure 1. The gradient was achieved by sputter-depositing the multilayer materials through a mask onto the rotating substrate, so that the time-averaged deposition gave the desired material thickness at each point on the mirror. The 32-nm reflectivity across the mirror was 45%, as measured at a synchrotron-based reflectometer [26]. Only X-rays within a bandwidth of 9 nm and which propagate from near the sample interaction point are efficiently reflected. Broadband plasma emission from the sample is filtered out by the resonant mirror. Also, off-axis radiation scattered from beamline components

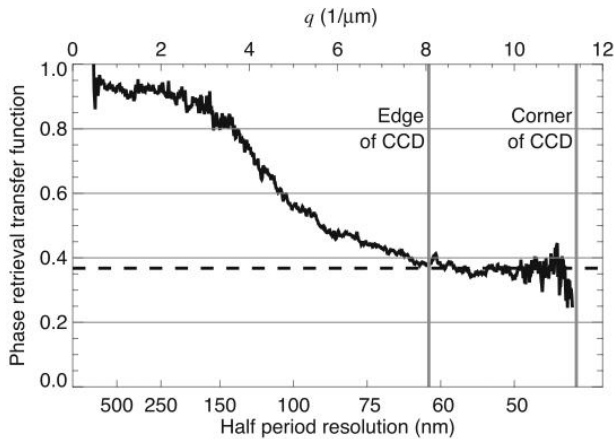


FIG. 4: The image is reconstructed to the diffraction limit. Phase-retrieval transfer function (PRTF) [9, 23] for the reconstructed image shown in Figure 3(b) and (d), averaged over shells of constant momentum transfer where is the wavelength and the diffracted angle. The PRTF is equal to unity when the phase is consistently retrieved and zero when the phase is unknown. Using the convention [23] that the resolution is given by the point where the PRTF drops to $1/e$, the resolution of our reconstruction is estimated to be 62 nm.

is reflected at less than 1% and hence filtered from the diffraction pattern. The reflectivity of the coating diminishes smoothly to zero close to the edge of the central hole, due to decoherence of the coating layers caused by the underlying substrate roughness where the hole was cored. This “soft edge” reduces scatter from the hole, whose shadow can be seen as a dark circle at the centre of the patterns in Figure 2. The on-axis path length of the reflected beam from the sample to the CCD was 55 mm, and for 32 nm radiation and objects smaller than 20 μm , this distance is in the far field, where the diffraction pattern is equal to the Fourier transform of the exit wave [27].

Image reconstruction was carried out with the Shrinkwrap algorithm [8]. Phase retrieval in Shrinkwrap is a non-linear optimization problem in a high-dimensional phase space. The dimensionality is equal to the number of phases to be retrieved: 1.7 million in this case. The solution is obtained iteratively by sequentially enforcing known constraints in diffraction and image spaces. We specifically aim for diffraction phases that are such that the waves re-interfering to form the image must all destructively cancel in areas outside the object’s boundary (called its support), and that the amplitudes of the discrete Fourier transform of the image match the measured diffraction amplitudes (which must be measured finely enough to include enough empty space beyond the object to constrain the phases). Other iterative transform algorithms usually require that the support of the object be known a priori, and the closer the support to the actual object boundary, the better the re-

construction. Shrinkwrap, however, periodically refines the support constraint from the current estimate of the image. The support constraint is calculated every 70 iterations by selecting pixels with intensity values greater than 0.2 times the maximum image intensity, after first blurring the image with a Gaussian kernel. The blurring kernel is initially set to 3 pixels full-width half-maximum (FWHM) and is gradually reduced to 0.7 pixels FWHM by iteration 5000. The final support is that found four update cycles prior to the point where the normalized image error [9] exceeds a value of 0.2. This stopping criterion is typically reached in 3000 to 4000 iterations. During the iterations we did not constrain the intensity or phase in the region in the mirror hole, which contains the unrecorded zero spatial frequency, nor did we constrain the object to be real or positive. We performed many reconstructions, starting each time from random phases. Each reconstructed image varied slightly due to the fact that with photon shot noise there is no true solution that exactly satisfies all constraint sets. However, each image determined from the final iterate was clearly recognizable as compared with the SEM image. The image estimate, displayed in Fig. 3 (b) and (d) is the average of 250 independent reconstructions.

ACKNOWLEDGEMENTS

Special thanks are due to the scientific and technical staff of FLASH at DESY, Hamburg, in particular to J. Feldhaus, R. L. Johnson, U. Hahn, T. Nuñez, K. Tiedtke, S. Toleikis, E. L. Saldin, E. A. Schneidmiller, and M. V. Yurkov. We also thank R. Falcone, M. Ahmed and T. Allison for discussions, J. Alameda, E. Gullikson, F. Dollar, T. McCarville, F. Weber, J. Crawford, C. Stockton, W. Moberlychan, M. Haro, A. Minor, H. Thomas and E. Eremina for technical help with these experiments. This work was supported by the following agencies: The U.S. Department of Energy (DOE) under Contract W-7405-Eng-48 to the University of California, Lawrence Livermore National Laboratory (the project 05-SI-003 was funded by the Laboratory Directed Research and Development Program at LLNL); The National Science Foundation Center for Biophotonics, University of California, Davis, under Cooperative Agreement PHY 0120999; The National Center for Electron Microscopy and the Advanced Light Source, Lawrence Berkeley Lab, under DOE Contract DE-AC02-05CH11231; Natural Sciences and Engineering Research Council of Canada (NSERC Postdoctoral Fellowship to MB); the U.S. Department of Energy Office of Science to the Stanford Linear Accelerator Center; the European Union (TUIXS); The Swedish Research Council; The Swedish Foundation for International Cooperation in Research and Higher Education; and The Swedish Foundation for Strategic Research.

Competing Financial Interests: The authors declare

that they have no competing financial interests.

* Electronic address: henry.chapman@llnl.gov

† Electronic address: janos.hajdu@xray.bmc.uu.se

- [1] Neutze, R. Wouts, R., van der Spoel, D. Weckert, E. & Hajdu, J. Potential for biomolecular imaging with femtosecond X-ray pulses. *Nature* 406, 752-757 (2000).
- [2] Jurek, Z., Faigel, G. & Tegze, M. Dynamics in a cluster under the influence of intense femtosecond hard x-ray pulses. *Euro. Phys. J. D* 29, 217-229 (2004).
- [3] Hau-Riege, S.P., London R.A. & Szöke, A. Dynamics of X-Ray Irradiated Biological Molecules. *Phys. Rev. E* 69, 051906 (2004).
- [4] Bergh, M, Timneanu, N.O. & van der Spoel, D. Model for the dynamics of a water cluster in an x-ray free electron laser beam. *Phys. Rev. E* 70, 051904 (2004).
- [5] Fienup, J. R. Phase retrieval algorithms-a comparison. *Appl. Opt.* 21, 2758-2769 (1982).
- [6] Sayre, D., Chapman, H. N. & Miao, J. On the extendibility of x-ray crystallography to noncrystals. *Acta Cryst. A* 54, 232-239 (1998).
- [7] Miao, J., Charalambous, P., Kirz, J. & Sayre, D. Extending the methodology of x-ray crystallography to allow imaging of micrometre-sized non-crystalline specimens. *Nature* 400, 342-344 (1999).
- [8] Marchesini, S. et al. X-ray image reconstruction from a diffraction pattern alone. *Phys. Rev. B* 68, 140101(R) (2003), arXiv:physics/0306174.
- [9] Chapman, H. N. et al. High-resolution ab initio three-dimensional X-ray diffraction microscopy. *J. Opt. Soc. Am. A* 23, 1179-1200 (2006), arXiv:physics/0509066.
- [10] Huld, G., Szöke, A. & Hajdu, J. Diffraction imaging of single particles and biomolecules. *J. Struct. Biol.* 144, 219-227 (2003).
- [11] Henderson, R. The potential and limitations of neutrons, electrons and X-rays for atomic resolution microscopy of unstained biological molecules. *Quart. Rev. Biophys.* 28 171-193 (1995).
- [12] Howells, M. R. et al. An assessment of the resolution limitation due to radiation-damage in x-ray diffraction microscopy, *J. Electr. Spect. Rel. Phenom.* (in press), arXiv:physics/0502059.
- [13] Persson, P., Lunell, S., Szöke, A., Ziaja, B. & Hajdu, J. Shake-up and shake-off excitations with associated electron losses in X-ray studies of proteins. *Protein Science* 10, 2480-2484 (2001).
- [14] Timneanu, N., Coleman, C., Hajdu, J. & van der Spoel, D. Auger Electron Cascades in Water and Ice. *Chemical Physics* 299, 277-283 (2004).
- [15] Ziaja, B., London, R.A. & Hajdu, J. Unified model of secondary electron cascades in diamond. *J. Appl. Phys.* 97, 064905 (2005).
- [16] Solem, J.C. & Baldwin, G.C. Microholography of living organisms. *Science* 218, 229-235 (1982).
- [17] Ayvazyan, V. et al. First operation of a free-electron laser generating GW power radiation at 32 nm wavelength. *Eur. Phys. J. D* 37, 297-303 (2006).
- [18] Saldin, E.L., Schneidmiller, E.A. & Yurkov, M. *The physics of free-electron lasers.* Springer, Berlin (2000).
- [19] Wolf, E. Three-dimensional structure determination of semi-transparent objects from holographic data. *Opt. Comm.* 1, 153-156 (1969).
- [20] Pfeifer M.A., Williams G.J., Vartanyants I.A., Harder, R. & Robinson, I. K. Three-dimensional mapping of a deformation field inside a nanocrystal. *Nature* 442, 63-66 (2006).
- [21] He, H. et al. Experimental lensless soft-x-ray imaging using iterative algorithms: phasing diffuse scattering. *Acta Cryst. A* 59, 143-152 (2003).
- [22] Miao, J. et al. Imaging whole *Escherichia coli* bacteria by using single particle x-ray diffraction. *Proc. Natl. Acad. Sci. USA* 100, 110-112 (2003).
- [23] Shapiro, D. et al. Biological imaging by soft x-ray diffraction microscopy. *Proc. Nat. Acad. Sci. USA* 102, 15343-15346 (2005).
- [24] Henke, B.L, Gullikson, E.M. & Davis J.C. X-ray interactions: photoabsorption, scattering, transmission, and reflection at E=50-30000 eV, Z=1-92. *At. Dat. Nucl. Dat. Tab.* 54, 181-342 (1993).
- [25] More, R. M., Warren, K. H., Young, D. A. & Zimmerman G. B. A new quotidian equation of state (QEOS) for hot dense matter. *Phys. Fluids* 31, 3059-3078 (1988).
- [26] Underwood, J.H. & Gullikson, E.M. High-resolution, high-flux, user friendly VLS beamline at the ALS for the 50-1300 eV energy region, *J. Electr. Spect. Rel. Phenom* 92, 265-272 (1998).
- [27] Goodman, J. W. *Statistical Optics.* John Wiley Sons (1985).